Dynamics of a hierarchical spin glass

1991 J. Phys. A: Math. Gen. 24 2625

(http://iopscience.iop.org/0305-4470/24/11/028)

J. Phys. A: Math. Gen. 24 (1991) 2625-2644. Printed in the UK

Dynamics of a hierarchical spin glass

R Riera† and J A Hertz

Nordita, Blegdamsvej 17, 2100 Copenhagen Ø, Denmark

Received 29 June 1990, in final form 7 February 1991

Abstract. We study the statics and long-time dynamics of a spin glass on a family of hierarchical lattices. The statics may be solved exactly on these lattices, and we treat the dynamics in a physically motivated low-temperature approximation, retaining only the slowest mode at each renormalization step. The results are generally in good agreement with Monte Carlo simulations in two and three dimensions. In particular, we find dynamical scaling at the spin glass transition in three dimensions, with a dynamical exponent $z = 6.5$. The spin autocorrelation function at T_g decays like t^{-x} with $x = 0.05$. A new result for statics which is used in the dynamics calculation is that for the magnetic exponent y_{eh} at the critical point, which is found to be 2.65. Above T_g, the autocorrelation function can be fit in a wide intermediate time range by a Kohlrausch form, but in this model this is only a consequence of a crossover in the renormalization flow and has no fundamental dynamical significance.

1. Introduction

Fifteen years after the introduction of the Edwards-Anderson (EA) model [1] opened the door to the theoretical development of the problem, short-range spin glasses remain an unsolved problem. For a few years now, it has been established that the three-dimensional (3D) Ising EA glass has a non-zero transition temperature T_g, while the two-dimensional (2D) model does not. However, it is still not known whether the spin glass state below T_g in three dimensions is a simple one, with a single thermodynamic phase (up to a global flip of all the spins) [2], or whether it exhibits non-trivial broken ergodicity like the infinite-range model [3]. Even with the assumption that the spin glass state is a simple one, no full theory exists, only a scaling theory [2, 4]. It is therefore very helpful to have some results on soluble models which may guide us in constructing theories for the EA model.

In this paper we study a model of a short-range Ising spin glass defined on a hierarchical (Berker) lattice [5]. Its statics can be solved exactly at all temperatures. Here we study its dynamics approximately at low temperature. The exact static solution on the hierarchical lattice is the same as the Migdal-Kadanoff bond-moving approximation [6, 7] on a Euclidean lattice. Within this correspondence, we may make comparisons with 2D and 3D lattice EA models.

The Migdal-Kadanoff approximation was shown a long time ago to give surprisingly good results for statics [8, 9]. Here we find within our approximation scheme that it is also very good for dynamics. Our work complements that of Bray and Moore [4] on the low-temperature phase; our focus is on $T \geq T_g$ in zero or small fields.

† Present address: Departamento de Física, Pontifícia Universidade Católica do Rio de Janeiro, Rua Marquês de São Vincente 225, 22453 Rio de Janeiro, Brazil.

0305-4470/91/112625+20$03.50

The qualitative features of the theory are already contained in a scaling theory proposed by McMillan [12]. However, the scaling theory only gave qualitative results, not explicit values of correlation functions or critical exponents. In the present model we can calculate all such quantities exactly. We obtain critical dynamics in good agreement with Monte Carlo simulations in $d = 2$ and 3. By tuning the parameters of the model suitably, we can also study the interesting case corresponding to the lower critical dimensionality.

A feature that arises not only in spin glasses, but also in a wide variety of other disordered systems, is anomalous relaxation. By this we mean relaxation which is neither simply exponential nor power-law in time, but something in between, often fit by the Kohlrausch form $\exp[-(t/\tau)^{\beta}]$. It turns out that the spin autocorrelation function we calculate can be fit by such a form (at appropriate temperatures) over many decades of time. However, this form has no fundamental significance in the present model. We will see that it is just a consequence of a slow crossover between power law and ordinary exponential decay.

Our model does not admit the possibility of non-trivial broken ergodicity (broken replica symmetry) [13]. Thus it may miss some important physics which recent simulations [14, 15] suggest is present in 3D spin glasses. However, in our view the current evidence on the existence of broken ergodicity is not conclusive because of possible large finite-size effects [4], so we find it still worthwhile to study the present model for insight about properties of spin glasses without broken ergodicity.

2. The model

We consider a short-range Ising spin-glass described by the Hamiltonian

$$\mathcal{H} = -\sum_{\langle ij \rangle} J_{ij} S_i S_j \tag{1}$$

with $S_i = \pm 1$ and Gaussian random nearest-neighbour exchange interactions satisfying (the brackets $[\ ]_{\mathrm{av}}$ denote the bond average)

$$[J_{ij}]_{\mathrm{av}} = 0 \qquad [J_{ij}^2]_{\mathrm{av}} = J^2. \tag{2}$$

The spins occupy a hierarchical lattice (figure 1) generated by the iterated replacement of a single bond by n bonds arranged in $n/2$ parallel 'rungs'. The fractal dimensionality of the lattice is $d_f = \ln n / \ln 2$. Its geometry allows exact computation of the partition

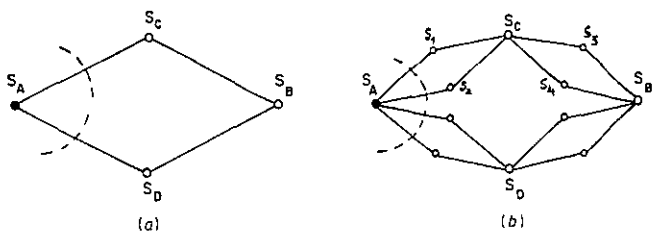

Figure 1. The $d = 2$ hierarchical lattice is constructed by the iterated replacement of each bond in (a) by one cell, as shown in (b). The renormalization step corresponds to the inverse transformation, in which the cell is replaced by an effective bond and the remaining spins have a new, slower, flip attempt rate because of barriers within the eliminated cell.

function (for fixed J_{ij}) by successive tracing over the different levels of spins in the hierarchy, starting from the last 'generation' and working back. For the random system, this renormalization procedure leads [8] to a nonlinear functional recursion relation for the effective bond distribution at a given length scale.

We adopt a single-spin-flip (Glauber) model for the dynamics [16]. Explicitly, the flip probability per unit time is

$$W(S_i \to -S_i) = \frac{1}{\tau_0} \frac{1}{1+\exp \beta(\delta E)_i} \tag{3}$$

where

$$(\delta E)_i = 2S_i \sum_j J_{ij} S_j \tag{4}$$

is the energy change for the flip $S_i \to -S_i$.

At each renormalization step, there emerges a new timescale τ_l that plays the role in the dynamics of the system at the corresponding lengthscale that τ_0 plays in the original lattice. The ratio τ_l/τ_{l-1} is greater than 1, reflecting the hindrance to free flipping of the remaining spins due to their interactions with the spins eliminated at the previous step.

Here we will always work within a low-temperature approximation, where (3) becomes

$$W(S_i \to -S_i) \approx \frac{1}{\tau_0} \exp(-\beta \max[(\delta E)_i, 0]). \tag{5}$$

3. Renormalization procedure

We start by reviewing the statics, that is the renormalization of the distribution of interactions J_{ij} [8, 9]. Referring to figure 1(a), we have that when we trace out the last-generation spins (ones with only two bonds connected to them) each pair of bonds (e.g. J_{AC}, J_{CB}) 'in series' combines to give an effective bond (J_{ACB}) according to

$$\tanh J_{ACB} = \tanh J_{AC} \tanh J_{CB}. \tag{6}$$

Then, the resulting effective bonds for the different parallel rungs add to give the new total effective bond between the spins at the ends of the original cell. For example, for the case $n = 4$ ($d = 2$) shown in figure 1(a), there are two rungs to add up, and we get

$$J' = J_{ACB} + J_{ADB}. \tag{7}$$

Now all the bonds that are combined in this way at the first renormalization step are drawn from the initial distribution of the model, which we take to be Gaussian. The distribution of the effective bonds after renormalization is no longer Gaussian. Following Southern and Young [9], we adopt Thouless's suggestion and find the new distribution at each renormalization step in the following way: We start with a large number N_0 of bond values sampled from the original distribution. We then take n of these at random and combine them as described above to get a renormalized bond.

Doing this N_0 times give a sample of N_0 values from the bond distribution at the first renormalization step. These numbers are then used in the same way to generate a corresponding sample of the distribution at the next step, and so forth. For large enough N_0 we can calculate any desired averages as averages over the sample distributions, and the distributions themselves can be plotted out by making histograms of the sample bonds. In our calculations we have used $N_0 = 20\,000$.

Now we turn to dynamics. After the last-generation spins have been eliminated, we have a new problem in which the spins of the next-to-last generation are the fastest degrees of freedom. Our task is to compute the effective spin-flip attempt rate, τ_1^{-1} for these spins. These spins will be slower than the last-generation ones because they are not really free to flip with rate τ_0^{-1}. Their couplings to the last-generation spins create barriers which hinder their free flipping. Since the last-generation spins are no longer in the problem explicitly, we must take their effect into account by a suitable renormalization of the flip attempt rate.

Actually, it is only an approximation to describe all the dynamical effects of the eliminated spins as a renormalization of the attempt rate. In general the eliminated spins have a spectrum of relaxation rates, and the exact renormalized dynamics should include the entire spectrum. What we de here is to keep systematically the slowest part of the dynamics at every renormalization step. At low temperatures, the slowest modes in the spectrum dominate exponentially, so we expect this single-parameter scaling to describe the dynamics in the long-time limit.

Our theory is based on the assumption that the timescales associated with different length scales (renormalization steps) are well separated from each other ($\tau_l \gg \tau_{l-1}$). We expect this to be a good approximation for temperatures well below the mean field transition temperature, where characteristic energies grow with increasing length-scale. In particular, it should give reasonable results even in the paramagnetic phase for dimensionalities d near or below the lower critical dimension d_l, as then the critical temperature is zero or small. For Ising spin glasses, $d_l \simeq 2.6$ [17, 18] permitting this approximation for $d = 2$ and $d = 3$.

Despite the physical appeal of this approximation procedure, we have not been able to justify it rigorously as a low-T expansion. The problem lies in the following: because at every renormalization step there is a distribution of relaxation modes, there is the possibility that a mode which is thrown away at one step (because it is not the slowest at that step) is actually slower than one which is retained because it is the slowest one at a later step. We have not succeeded in bounding the error introduced in this way, even for the one-dimensional case. For the present, we are forced to regard our scheme as a heuristic one which we believe captures the correct physics of the problem at low temperatures, though it may not be quantitatively exact.

To compute the renormalized attempt rate, we examine in detail just how next-to-last-generation spins can relax. Consider, specifically, the pair of neighbouring last-generation cells formed by spins S_A, S_B, S_C, S_1, S_2, S_3 and S_4 shown in figure 1(b). S_1, S_2, S_3 and S_4 are last-generation spins which are to be eliminated at this renormalization step. S_C is the next-to-last-generation spin whose dynamics we are examining. S_A and S_B belong to earlier generations and are effectively frozen on the timescales we are examining here.

Let us consider the relaxation of this system to equilibrium. On a timescale τ_0, S_A, S_B and S_C are all frozen and simply act, via the bonds within the last-generation cells, as sources of external fields acting on the last-generation spins S_1, S_2, S_3 and S_4. So the first thing that will happen is that these spins will line up along the net fields they

feel. The result of this alignment will be that if the fields coming from the two end spins (S_A and S_C for S_1 and S_2, S_B and S_C for S_3 and S_4) are of opposite sign, a last-generation spin will follow the one associated with the stronger bond, leaving the other bond broken. Now this may or may not leave the two elementary cells in their lowest-energy states. In the present example, an unfrustrated cell (one with an even number of negative bonds) will be in its ground state if all its bonds are satisfied, and a frustrated cell (one with an odd number of negative bonds) will be in its ground state if only the weakest bond is broken. Examples of cells not in their ground states are unfrustrated cells with broken bonds in both the top and bottom rungs (since they cannot relax to their ground states without flipping an end spin) and frustrated cells where the broken bond is in the top rung, while the weakest bond of all is one of the bottom pair (or reversing top and bottom).

On the next timescale, where these cells are replaced by bonds (which are calculated by the static renormalization procedure outlined above) S_C can relax. It is sufficient for illustrative purposes to consider the case where, say the left-hand cell in figure 1(*b*) (containing S_1 and S_2) is not in its ground state, while the right-hand cell (containing S_3 and S_4) is, but the total energy would be lower if it were the right-hand one in its ground state instead. If we can flip S_C, both cells will immediately relax to that lower-energy configuration. The question is, what is the barrier for flipping S_C?

One possibility is that S_C can just flip, breaking any unbroken bonds and unbreaking any broken bonds connected to it. The barrier associated with this is just twice the sum of the (absolute values of the) bonds which are broken in the flip, minus the sum of those previously broken which are unbroken after the flip.

Another possibility, however, is that S_1 or S_2 (or both) might flip briefly, changing the state (broken or unbroken) of the bonds in the upper or lower rung (or both of them) in the left-hand cell, and then S_C flips. Because the rate for this process will be suppressed by the small probability of these fluctuations, the effective total barrier will be correspondingly increased. On the other hand, the subsequent flip of S_C will be easier if the flips of S_1 and/or S_2 happen to break bonds connected to S_C, for then the flip of S_C will change these bonds from broken to unbroken, thus lowering the energy associated with them.

In general, then, we have to consider all possible sequences of flips of a set of spins consisting of the central spin (S_C) and the spins in the cell of higher initial energy (here, S_1 and S_2). We can think of this process as moving a domain wall through the pair of cells. The total barrier for each such sequence is the sum of the activation energies $V_i = \max(\delta E_i, 0)$ for these flips:

$$V_s = \sum_i V_{i,s} \tag{8}$$

where s labels the different possible sequences. We then compare the total barriers for different sequences and select the smallest one:

$$V_1 = \min_s V_s. \tag{9}$$

At low temperatures, this path will dominate all others. The renormalized flip attempt rate is therefore

$$\tau_1^{-1} = \tau_0^{-1} \exp(-\beta V_1). \tag{10}$$

Similarly, at every subsequent step, the relaxation time is multiplied by the inverse of

a factor like (10), leading to

$$\tau_l = \tau_0 \exp(\beta \Delta_l) \tag{11}$$

where the total barrier after l steps is

$$\Delta_l = \sum_{m=1}^{l} V_m. \tag{12}$$

Thus we can think equally well in terms of a multiplicative renormalization of timescales or an additive contribution to the effective barriers at each renormalization step.

Frustration can play an important role in the energies that come out of this computation, and consequently in the scaling of the characteristic relaxation times of the system. This is illustrated in figure 2. It shows two different intra-cell bond configurations, in both of which the minimum coupling is J_1, located at bond 1. Figure 2(a) shows the barrier calculation (8) for a sequence of spin-flips in the first bond configuration, where all the couplings are ferromagnetic (no frustration in the ground-state of the cell). Figure 2(b) shows the barrier calculation for the same sequence of spin-flips in a second cell where all the bonds have the same strength as in (a), but bond 1 is antiferromagnetic. Here, because of frustration, the ground state energy of the cell is $\Delta E_0 = 2|J_1|$ higher than in the previous case. The effective barrier V_s for the relaxation sequence shown in the figure is also higher in the second case. This illustrates how frustration can lead to higher barriers.

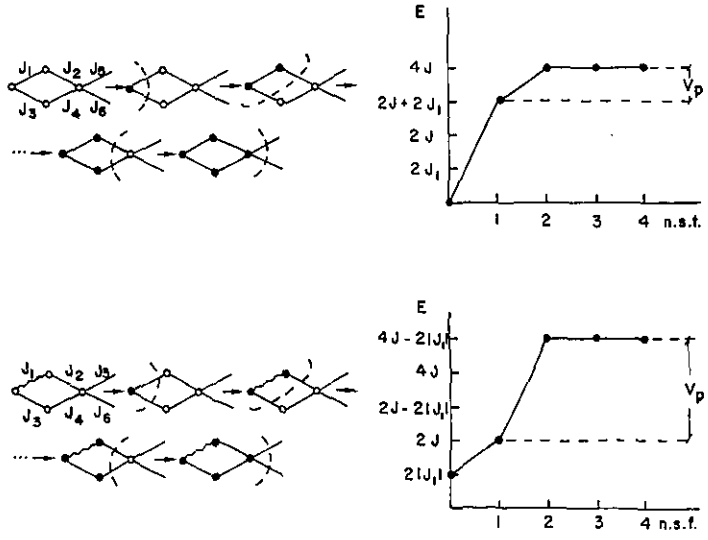

Figure 2. Illustration of the effect of frustration on barrier calculations. Two different intracell bond configurations are shown, one without and the other with frustration. The sequence of spin flips is the same for both cases. The 'domain wall' (dotted line) moves as the spins are flipped (full circles). For simplicity, the two intracell bond configurations are taken to have $J_2 = J_3 = J_4 = J_5 = J_6 = J$ and $|J_1| = \frac{1}{2}J$. In (a), $J_1 > 0$, and there is no frustration in the ground state of the cell. In (b), $J_1 < 0$, and the ground state is frustrated, with bond 1 unsatisfied (wiggly line). Here the domain wall should be understood as relative to the ground state configuration. The energy is plotted for both cases against the number of spin flips (nsf). At nsf = 0, the energy corresponds to the ground state. The barrier V_s for the given sequence of flips is the sum of the positive energy changes after the wall was created by the flip of the left-hand spin at nfs = 1.

The generalization to lattices with more than two rungs per cell is straightforward. We note two simplifying features. First, in considering different subsequences of flips of the internal spins during which the 'central spin' at one end of the cell (S_C, in our example) does not flip, the order of flipping of the internal spins is irrelevant. This is because in the geometry of the present model, the flips of different internal spins just make independent contributions to the barrier. Second, once the central spin flips, the cell can relax to its ground state in a microscopic time (τ_0). So only the flips of internal spins *before* the flip of the central spin contribute to the barrier.

Of course, since the interactions are random, the resulting barrier increases or timescale renormalizations will also be random, and we must study their distribution. We do this in the same way we follow the renormalization of the bond distribution in the static calculation—we construct many examples of pairs of adjacent cells from the bond distribution at the previous renormalization step, and for each one compute a V_l. The list of these V_l's then provides a sample of the distribution of barrier increases at this step.

With the above considerations, we state the complete step l of the dynamic renormalization procedure as:

(i) Take the previous distributions of N values of exchange interactions $P_{l-1}(J)$ and barriers $G_{l-1}(\Delta)$.

(ii) Choose randomly n values from the bond distribution to construct one cell at the last remaining generation. (In the case of the cell of figure 1, $n=4$.)

(iii) Find the renormalized interaction J_l by the standard real space renormalization procedure outlined above.

(iv) Choose randomly $2n$ values from the interaction distribution to construct a pair of adjacent cells in the last remaining generation.

(v) Fixing the spins at the ends of the cells randomly, find their minimum-energy configuration. Compute the path barriers for all possible sequences of flipping the central spin and the internal spins in the cell of higher energy according to (8). Then the smallest of these (9) will give one value for the effective barrier increase V_l at this step.

(vi) Choose (randomly) one value of Δ_{l-1} from the previous barrier distribution. The renormalized barrier will be given by

$$\Delta_l = \Delta_{l-1} + V_l. \tag{13}$$

(vii) Repeat the previous items N times to obtain the renormalized distributions $P_l(J)$ and $G_l(\Delta)$, which will be used as starting distributions in the next RG step

The only approximation present so far is the one mentioned above: keeping only one characteristic time (the longest) in the true renormalized dynamical spectrum at every renormalization step. (The non-zero width of the barrier distribution obtained in our procedure comes about because of the quenched randomness of the system.) As argued there, this should be a good approximation for long times at low temperature. In particular, the shape of the resulting barrier distributions should (if calculated correctly) lead to the long-time limiting form of correlation functions characteristic of the Griffiths phase [10]. (This is analogous to the case of the *static* Griffiths singularities as a function of field described by Grinstein *et al* [11] for the spin glass chain.)

The starting interaction distribution (2) remains symmetric through the successive rescalings, and the static properties are obtained from the scaling behaviour of the width of the distribution [8]. The critical temperature T_g is characterized by an unstable fixed point exchange distribution $P^*(J)$. At T_g, there is also a fixed point distribution

of barrier increments V_l, leading to effective growing barriers Δ_l (12) with a distribution increasingly narrow relative to its mean as the length scale is increased.

This is also approximately the case above T_g when the correlation length $\xi \gg 1$, i.e. as long as there are many RG steps before the barrier saturates at a scale $L = 2^l \simeq \xi$ (where J_l or $V_l \simeq 0$). The dynamic properties will then be dominated by the scaling properties of the mean of the barrier distribution. In this paper, we will make the further approximation (in addition to that mentioned above) of ignoring fluctuations around the mean, replacing V_l by its mean $\bar{V}_l$ at each step. Thus, at T_g,

$$\tau_l \propto (\exp \beta V^* l) \tag{14}$$

where V^* is the mean of the fixed point distribution of barrier increments. Away from T_g we have, correspondingly,

$$\tau_l = \tau_0 \exp\left(\beta \sum_{m=1}^{l} \bar{V}_m\right) \tag{15}$$

where $\bar{V}_m$ is the average barrier increment at step m.

Because of this last approximation, we can never hope to see the Griffiths-phase long-time limiting form of the correlation function in our subsequent calculations. Thus we have to qualify our claim to a good long-time theory with the proviso 'apart from effects of Griffiths singularities'. We expect these effects to be very small, however, in the region near T_g which we are most interested in, because there the mean effective barrier is much larger than its fluctuations.

Although the dynamics is governed by the scaling of the barrier distribution, the change V_l depends on the exchange distribution at the previous level $l-1$. For that reason, the dynamic transition will always occur at the critical point for statics, in contrast to the results of Kutasov *et al* [19] for an Ising chain with a hierarchical distribution of couplings.

4. Results for hierarchical lattices

We consider the hierarchical lattices generated by the iterated substitution of a single bond by a generator with n bonds and $n/2$ rungs, as in figure 1. In addition to $n = 4$ (corresponding to $d = 2$) and $n = 8$ (corresponding to $d = 3$) we can do calculations for non-integer dimensions. For example, the case $n = 6$ ($d \simeq 2.58$) is particularly interesting because it is very close to the lower critical dimensionality.

We have worked with distributions of $N = 20\,000$ values and followed the flow of the distributions of effective exchange interactions and energy barriers through rescaling. For $T \to 0$, the exchange distribution approaches a fixed shape with a length-dependent scale ($b = 2$):

$$P_l(J) = b^{-y_0} P_{l-1}(b^{-y_0} J) \tag{16}$$

with the width of the distribution scaling as ($\tilde{J}_l^2 = [J_l^2]_{\text{av}}$)

$$\tilde{J}_l = b^{y_0} \tilde{J}_{l-1}. \tag{17}$$

We find exponents $y_0 \simeq -0.27$ ($n = 4$, $d_f = 2$), $y_0 \simeq 0.04$ ($n = 6$, $d_f \simeq 2.58$) and $y_0 \simeq 0.25$ ($n = 8$, $d_f = 3$), in agreement with the results of Bray and Moore [17] for these lattices.

We also obtain for the distribution of barrier increments V_l at $T \to 0$

$$F_l(V) = b^{-y_0 l} f(b^{-y_0 l} V). \tag{18}$$

The mean $\bar{V}_l$ scales like

$$\bar{V}_l = b^{y_0}\bar{V}_{l-1} \tag{19}$$

with $\bar{V}_l = [V_l]_{\rm av}$ computed as the average of (9) over all N intra-cell bond configurations generated at step l. The exponents y_0 are the same as in (16) and (17), because V_l depends only on the intra-cell bonds that are sampled from the interaction distribution (16) at the previous level $l-1$. Figure 3 shows the zero-T scaling function f in (18) for $d=2$ and $d=3$.

There is no spin-glass order for finite T in $d=2$ ($y_0<0$). Near $T_g=0$, we can add increments (19) as in (15) until the barrier saturates at the value Δ_∞ for $l=\log_b \xi$. We then have

$$(\Delta_\infty - \Delta_l) = b^{y_0}(\Delta_\infty - \Delta_{l-1}) \tag{20}$$

or, equivalently, with $L=b^l$:

$$\Delta_\infty - \Delta(L) \sim L^{y_0}. \tag{21}$$

That is, in $d=2$ as $T\to 0$ the barriers saturate at large scales, approaching Δ_∞ with the zero-temperature exponent y_0 [12]. The saturation value depends linearly on temperature, while the width of the barrier distribution stabilizes at a fixed value, as shown in figure 4. The zero-temperature saturation value is $\Delta_\infty \approx 15J$, in qualitative agreement with cluster-quench simulations [20] which gave $\Delta_\infty \approx 12J$.

For $d=3$, $T_g>0$, and the spin-glass phase is governed at large length scale L by the $T=0$ fixed point interaction distribution. In this limit, the last contribution V_l to Δ_l in (15) dominates, so the energy barriers scale with the same (3D) exponent y_0 as the interactions

$$\Delta(L) = A(T)L^{y_0}. \tag{22}$$

This means that for this model the exponent Ψ introduced by Fisher and Huse [2] is equal to y_0.

The lower critical dimension is characterized by a zero-temperature exponent $y_0=0$. This case was approximated within the present model as follows. We started with the case $n=6$ (like figure 1 but with three rungs instead of two, and dimension $d_f \approx 2.58$). It is almost at lower critical dimensionality, but has a slightly positive y_0. We retarded the flow of the exchange distribution just enough to compensate for this, producing a fixed distribution by multiplying all the bonds found at each step by b^{-y_0}.

For $T\approx 0$, we find a temperature-independent value $\bar{V}_l = 3.1J$ for several RG steps before the correlation length is reached. This means that for a wide range of length scales the characteristic time (15) increases like

$$\tau_l = \tau_0 \exp(3.1\beta J l). \tag{23}$$

This implies a breakdown of the conventional dynamic scaling relation

$$\tau(L) \sim L^z \tag{24}$$

since (with $L=2^l$) the dynamic exponent

$$z = \frac{3.1\beta J}{\ln 2} \approx 4.5\beta J \tag{25}$$

is temperature-dependent.

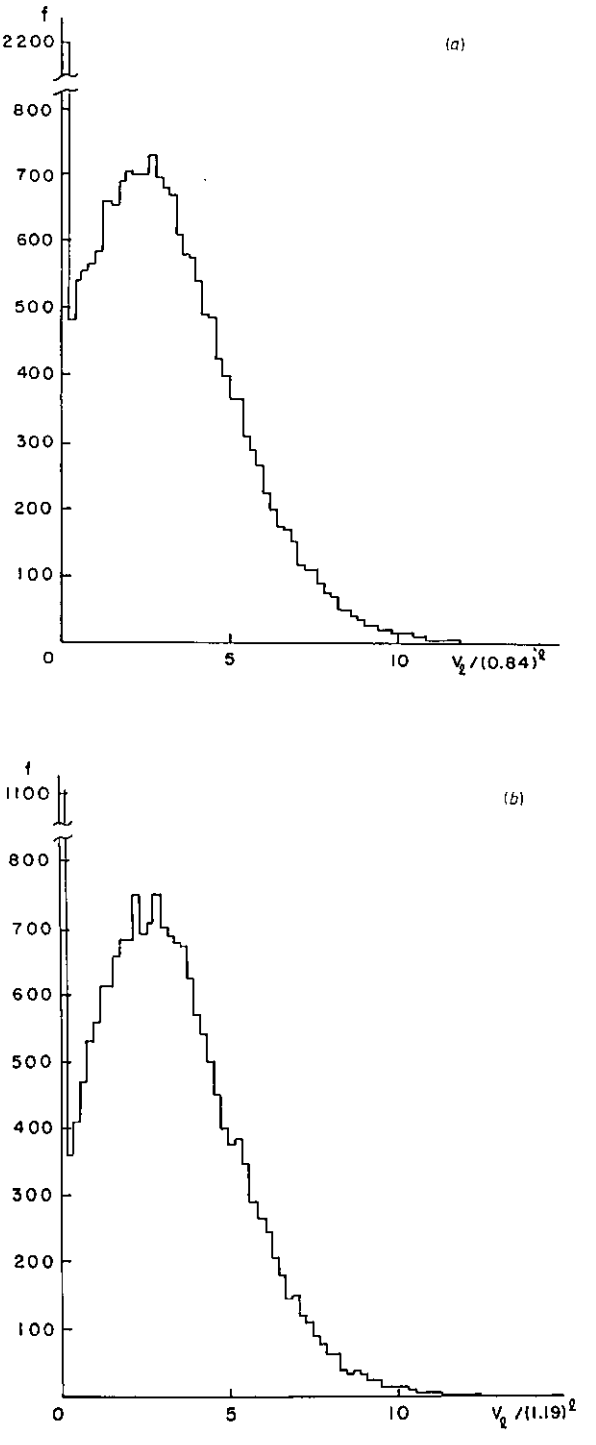

Figure 3. Histogram of the zero-temperature scaling function f for the distribution of barrier increments V_l (see text). It has 20 000 values of rescaled barriers $2^{-ly_0}V_l$ obtained at the lth renormalization step. (a): $d=2$. (b): $d=3$. In (a) the peak at $V_l=0$ contains approximately 10% of the total number of barrier increments generated; in (b), 5%.

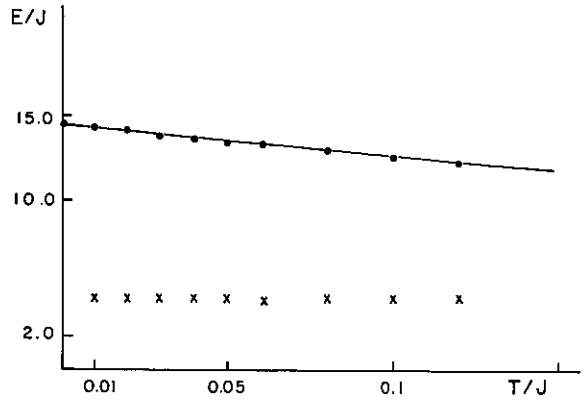

Figure 4. Plot of the mean (●) and width (×) of the distribution of barriers $\Delta_\infty(T)$ for the $d=2$ hierarchical lattice. The linear dependence at $T\to 0$ of $\Delta_\infty(T)$ is $\Delta_\infty(T)=\Delta_\infty(0)-18.3T$, with $\Delta_\infty(0)=14.6J$.

Furthermore, by counting the number of RG steps l_ξ to achieve $\tilde{J}_l \simeq 0$ at low temperatures, we obtain for the correlation length $\xi_T = 2^{l_\xi}$ a behaviour consistent with (see figure 5):

$$\xi(T) \sim \exp[(0.8\beta J)^2] \tag{26}$$

in agreement with the scaling theory [12].

For $d=3$, the critical temperature obtained was $T_g/J \simeq 0.86 \pm 0.01$, and the thermal exponent $y_T = 0.36 \pm 0.04$. These results were obtained by following the flow of the

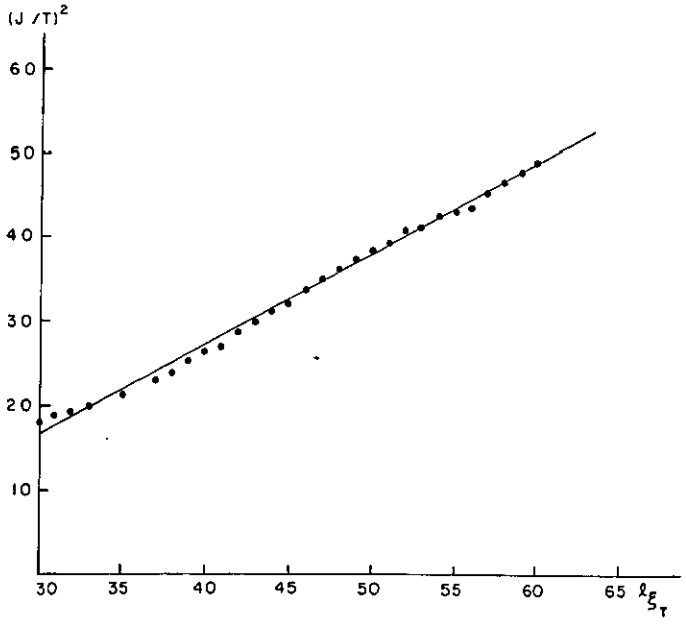

Figure 5. Correlation length at the lower critical dimensionality. Plot of $(J/T)^2$ against number of renormalization steps l_{ξ_T} necessary to reach the correlation length at low temperatures $T \leq 0.23J$. The result is consistent with $(J/T)^2 - C = l_{\xi_T} - l_{\xi_{0.23}}$ with $C = (J/0.23)^2$. From $l_{\xi_T}/l_{\xi_{0.23}} = 2^{l_{\xi_T} - l_{\xi_{0.23}}}$ we obtain $\xi_T \propto 2^{(J/T)^2}$ or $\xi_T \propto \exp[(J/T)^2 \ln 2]$.

interaction distribution and agree with previous results for statics [8], where the thermal exponent was obtained assuming that the exchange distribution remained Gaussian through the rescalings. Apparently this is a good approximation.

At T_g, (9) was evaluated at each step with intra-cell bond configurations sampled from the unstable fixed point interaction distribution. Then from (14) we obtain

$$\tau(L) \propto L^{V^*/T_g \ln 2} \tag{27}$$

at T_g, while for $T \geqslant T_g$ we get

$$\tau(T) = \tau_\infty \sim \tau_{l_\xi} \propto \xi^z. \tag{28}$$

Together, (27) and (28) indicate conventional dynamic scaling (24) with a dynamic exponent

$$z = V^*/T_g \ln 2. \tag{29}$$

From the measured fixed point distribution $F^*(V)$, we find the mean $V^* = (3.9 \pm 0.1)J$. Using this result in (29), we obtain the value

$$z = 6.5 \pm 0.1 \tag{30}$$

in very good agreement with Monte Carlo simulations [21] where $z = 6.0 \pm 0.8$ was found.

5. Dynamic correlation function

In this section we consider the behaviour in the high temperature phase of the dynamic correlation function $q(t) = [\langle S_i(0) S_i(t) \rangle]_{\text{av}}$ (the brackets $\langle\ \rangle$ denote the thermal average). In the limit $t \to \infty$, $q(t)$ is equal to the EA spin-glass order parameter for statics. This autocorrelation function can be written as [12]

$$q(t) = \sum_{l=0}^{\infty} \rho_l \mu_l^2 \exp(-t/\tau_l) \tag{31}$$

where ρ_l describes the fraction of active spins relaxing at a rate τ_l^{-1}, and μ_l is their effective magnetic moment.

In the hierarchical lattices studied here, $\rho_l \sim 2^{-dl}$, the fraction of sites which are traced over at step l of the renormalization. The magnetic moments μ_l at level l are obtained from the scaling exponent for the variance Δ_h of an infinitesimal random field applied to the system:

$$\Delta_{hl} = 2^{y_h} \Delta_{h,l-1} \tag{32}$$

or

$$\mu_l^2 = \mu_0^2 2^{l y_h}. \tag{33}$$

At $T = 0$, $y_h = d$ and for a small T_g, we expect a critical magnetic exponent y_{ch} slightly smaller than d. The explicit calculation of y_{ch} for hierarchical lattices is given in the appendix. In particular, we find the value

$$y_{ch} = 2.65 \tag{34}$$

for $d = 3$ at the critical point.

Using the l-dependence of p_l and μ_l, $q(t)$ reads

$$q(t) \propto \sum_{l=0}^{\infty} 2^{-l(d-y_h)} \exp(-t/\tau_l). \tag{35}$$

We now consider $d = 3$. At T_g, using (27), we get

$$q(t) \propto \sum_{l=0}^{\infty} 2^{-l(d-y_{ch})} \exp(-t/\tau_0' 2^{lz}) \tag{36}$$

where τ_0' is independent of l.

Transforming the sum into an integral and using steepest descent, (36) leads to the algebraic behaviour

$$q(t) \propto (\tau_0'/t)^x \tag{37}$$

with

$$x = \frac{d - y_{ch}}{z}. \tag{38}$$

Substituting the values of y_{ch} from (34) and z from (30) in (38), we obtain the critical exponent $x \simeq 0.05$, in very good agreement with Monte Carlo results [21].

For temperatures above T_g, the behaviour of the effective barriers with length scale was followed numerically (see figure 6). Before the barriers saturate, we found two regimes. Initially (at short length and time scales), they behave like

$$\beta \Delta_l = A(T) l \tag{39}$$

or

$$\tau_l \sim 2^{lz_{\text{eff}}(T)} = L^{z_{\text{eff}}(T)} \tag{40}$$

with $z_{\text{eff}} = A(T)/\ln 2$, in analogy with expression (29) at T_g. Steepest descent leads again to algebraic decay like (37), with an exponent x which is temperature-dependent through both y_h and z_{eff}.

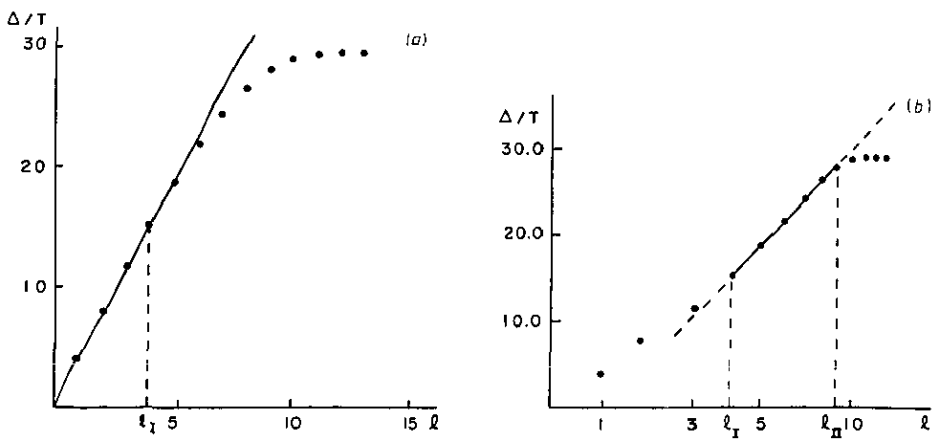

Figure 6. Renormalization of barriers ($d = 3$, $T = J$). Plot of Δ_l/T against (a) number of renormalization steps l and (b) $\log_{10} l$. The steps $l_I = 4$ and $l_{II} = 9$ separate approximately the linear, logarithmic, and saturation regimes.

In the second regime (intermediate timescales), we can make an approximate fit

$$\beta\Delta_l \approx B \ln l + C \tag{41}$$

or

$$\tau_l/\tau' \propto l^B \tag{42}$$

with $\tau' \sim 2^{zl'}$ being the initial timescale for this regime. Substitution of (42) into (35) leads to

$$q(t) \propto q(\tau') \sum_{l=l'}^{l_\xi} 2^{-l(d-y_h)} \exp(-t/\tau' l^B). \tag{43}$$

Applying steepest descent to (43), we obtain the Kohlrausch behaviour

$$q(t) \propto \exp[-(t/\tau')^{\tilde{\beta}}] \tag{44}$$

with a temperature-dependent exponent $\tilde{\beta} = 1/(1+B) \leqslant 1$, through the temperature dependence of B.

Some kind of region characterized by (41) is always to be expected if we consider Δ as a function of $u = \ln l$ instead of l. Then the initial (critical) behaviour is exponential in u, so the graph of $\Delta(u)$ curves upward for small u. Since it has to saturate at large u, it must go through an inflection point somewhere in between, and in this region a linear (i.e. logarithmic in l) fit will be good. This region may not be very large in l, but due to the large dynamical exponent z, which sets the scale for variations of Δ with l, this can correspond to many decades of t. Needless to say, however, the resulting Kohlrausch decay admits no interpretation in terms of particular special kinds of dynamical processes in the present model.

For length scales greater than ξ, the dynamics is governed by the slowest modes, which have $\tau_l \simeq \tau_\xi$. At such timescales we recover the usual long time exponential behaviour

$$q(t) \propto \exp(-t/\tau_\xi). \tag{45}$$

The true long-time behaviour of $q(t)$ in the presence of bond randomness exhibits effects of Griffiths singularities [10]. As pointed out above, these can be described within our theoretical framework if the full barrier distribution is calculated exactly, but we have not done this here. Because we were most interested in the neighbourhood of the phase transition, we made the approximation (15), arguing that corrections due to the finite width of the barrier distribution should not be significant close to the critical point. While we have not tried to estimate the (presumably very long) time where the Griffiths-phase behaviour takes over, we note that there is no sign of such behaviour in the simulations with which we have compared our results [21].

We also computed directly the expression (35) for $q(t)$ at $T \geqslant T_g$, with the exponent $y_h(T)$ evaluated from (A7). Figure 7 shows examples of plots of $q(t)$ which exhibit a crossover from the short-time power-law form to the intermediate-time Kohlrausch behaviour for $T > T_g$. The exponents extracted from such plots are shown in figures 8 and 9 and agree with the steepest descent results (37), (44) and (45). The approximate linear variation of $\ln\ln q$ with $\ln t$, which is the basis of the Kohlrausch fit, apparently works over a somewhat wider range than what we would expect from the width of the linear region in plots of Δ_l against $\log l$ like figure 6(b). This should make us even more cautious about attributing fundamental significance to Kohlrausch law fits.

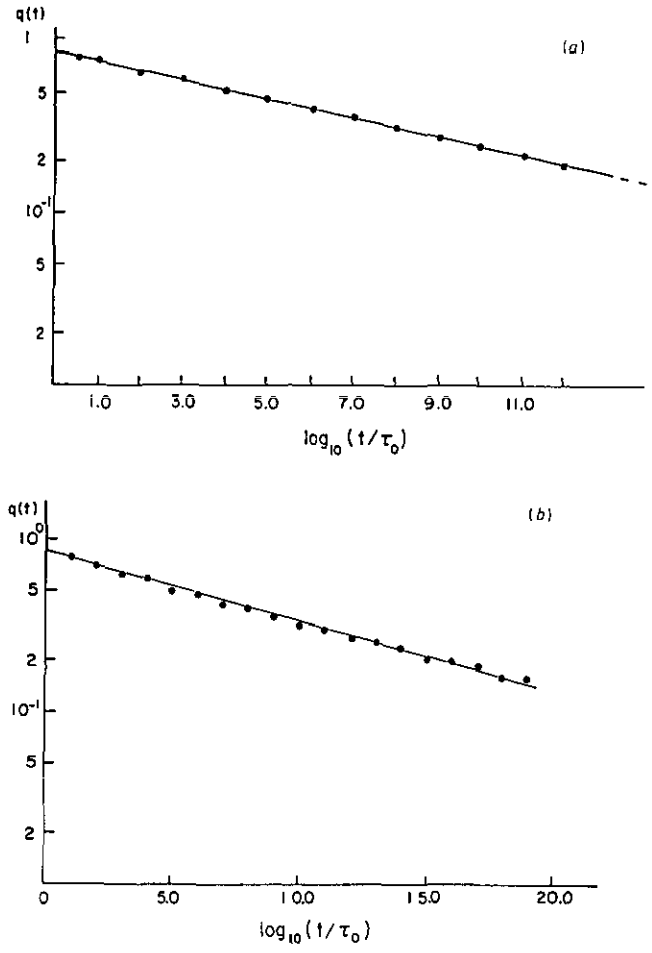

Figure 7. Dynamic correlation functions $q(t)$ for (*a*) $T = T_x = 0.89J$, (*b*) $T = 0.8J$ (*c* and *d*) $T = 1.0J$. (*a*), (*b*) and (*c*) exhibit the algebraic behaviour $q(t) \propto t^{-x}$, with $x = 0.054$, 0.04 and 0.073, respectively. (*d*) shows the intermediate Kohlrausch behaviour $q(t) \propto \exp[-(t/\tau)^{\bar{\beta}}]$ with $\bar{\beta} = 0.06$ (the straight line has slope $1 - \bar{\beta}$). Note that the timescales for this regime ($6 \leq \log_{10}(t/\tau) \leq 12$) correspond to the barrier range $14 \leq \Delta/T \leq 28$ of figure 6(*b*).

The exponent x is in good agreement with Monte Carlo simulations [21]. The low $\bar{\beta}$-values obtained are at least partially due to the failure of the low-temperature approximation in describing the larger length-scale effective spins in the paramagnetic phase because they are attained at higher temperatures along the RG process. Nevertheless, the present theory gives the correct qualitative behaviour of $q(t)$ for the intermediate regime as well as the observed linear temperature dependence of $\bar{\beta}$.

Our results suggest a crossover between the first two regimes rather than the combined behaviour $q(t) \sim t^{-x} \exp - ct^{\bar{\beta}}$ suggested by Ogielski [21].

For the 2D system, we also expect to find a crossover from linear barrier growth to saturation which can be fit by a logarithmic l-dependence. We have also verified that direct evaluation of the autocorrelation function (35) for $n = 4$ ($d_f = 2$) also permits a Kohlrausch fit for an intermediate time regime or temperature range like that shown for the 3D case in figure 7(*d*).

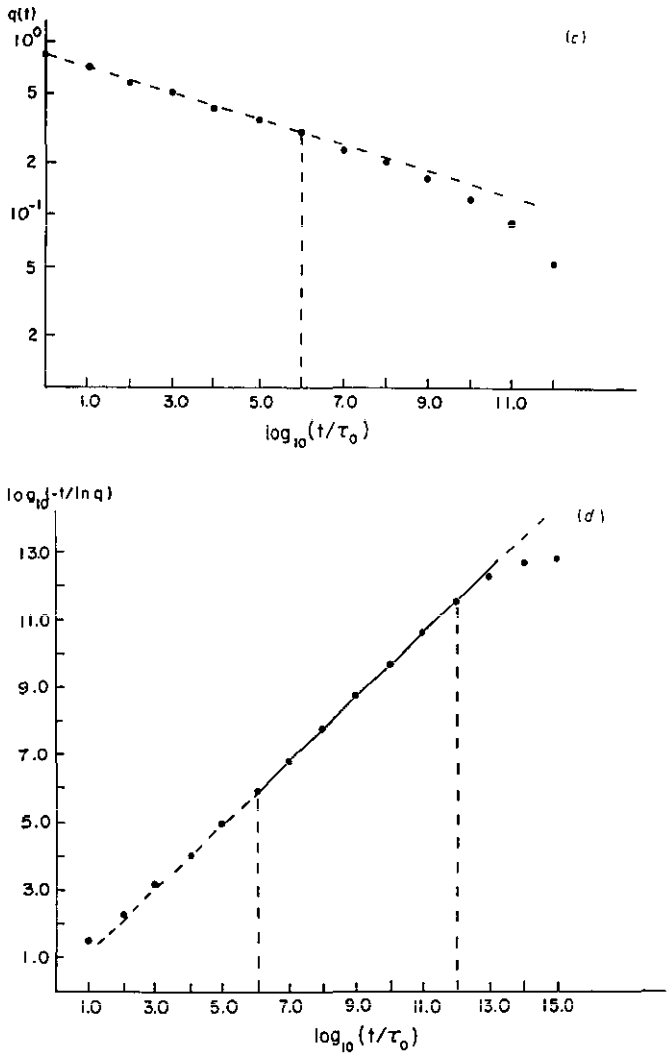

Figure 7. (continued)

6. Conclusions

We have studied the low-temperature dynamics of a soluble short-range spin glass: the Gaussian Ising model on a Berker lattice. The static properties are obtained exactly; for dynamics we are forced to an approximation in which only the slowest relaxation mode is kept at each renormalization step. While this is not exact (or even, to our knowledge, a systematic low-temperature approximation), the results resemble to a surprising degree those found in simulations of the corresponding model on a Euclidean lattice. We even find quantitative agreement for the characteristic exponents y_0, z, x and y_{ch}. (Though the last of these is a statics exponent, it does not seem to have been calculated before.)

Beyond exponents, we find that in the paramagnetic phase the autocorrelation function can be fit over a wide range of times by the popular Kohlrausch form. However,

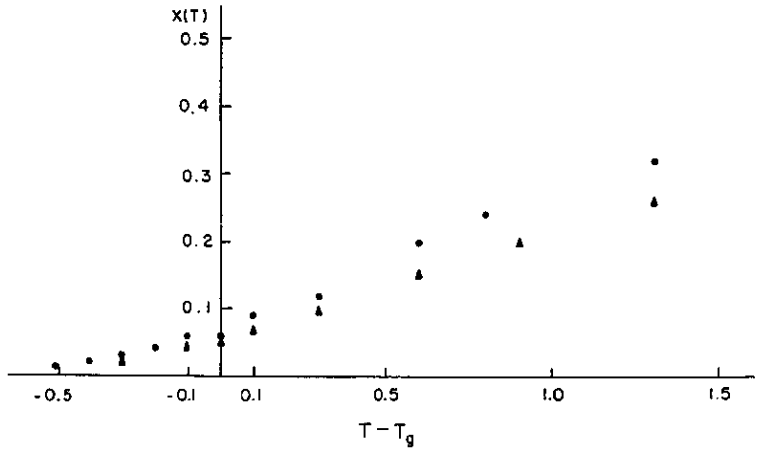

Figure 8. Temperature dependence of the exponent x for the algebraic decay $q(t) \propto t^{-x}$ obtained with the present method (▲). For comparison, we also plot the Monte Carlo results [21] (●).

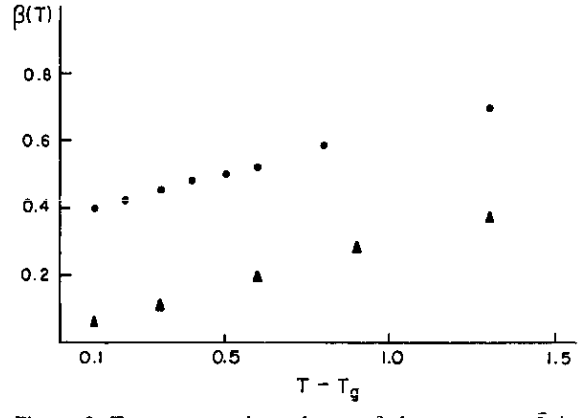

Figure 9. Temperature dependence of the exponent $\bar{\beta}$ in the Kohlrausch fit $q(t) \propto \exp[-(t/\tau)^{\bar{\beta}}]$. We plot (▲) for our results and (●) for the Monte Carlo ones [21].

as we have explained, this is not a reflection of some particular glassy processes occurring on these timescales. It arises in this model simply from two facts: (i) There has to be a region in the neighbourhood of the inflection point in the graph of the renormalized barrier Δ as a function of $\ln l$ where Δ varies approximately linearly with $\ln l$. (ii) The slope $\mathrm{d}\Delta/\mathrm{d} \ln l \approx l_c z_{\mathrm{eff}}$ (where l_c is the value of l at the inflection point) happens to be large. Thus a few decades of spatial scale correspond to many decades in time.

We think this result should encourage caution in the interpretation of data which can be fit by a Kohlrausch law.

Not all our exponents are in agreement with the simulations. The Kohlrausch exponent $\bar{\beta}$ is much too small (though its linear temperature variation is qualitatively correct). It is hard to account for all of this discrepancy simply in terms of the gradual breakdown of the low-temperature approximation we have used throughout this treatment, because the largest relative error occurs at low T. Thus there could well be other

sources of Kohlrausch behaviour, present in the lattice model for which the simulations were done but absent in our hierarchical model, or even present in our model but neglected in our treatment.

The thermal critical exponent y_T in three dimensions (which we obtained in confirmation of the old work of Southern and Young [9] for statics) is also in strong apparent disagreement with the simulations. (We find $\nu = y_T^{-1} \approx 2.8$, while Ogielski [21] has $\nu \approx 1.3$.) Indeed, a small value of y_T, close to the zero-temperature exponent y_0 (such as we find), is a natural consequence of proximity to the lower critical dimensionality. The fairly low value of T_g relative to its mean field value ($T_g/T_g^{\mathrm{MF}} \approx 0.36$) is also consistent with the idea that the 3D model is close to lower critical dimensionality. In this light the much larger value of y_T found in the simulations is something of a puzzle, suggesting that some new physics missed in the present model may be playing a major role in the real 3D system.

As we remarked in the introduction, recent simulations [15] (reported after most of our work was done) suggest the presence of broken ergodicity in the 3D Ising glass. In this light, it would be desirable to construct soluble models similar to ours but which allow many thermodynamic phases. This problem is under study. For the present, however, in view of the inconclusive nature of the present evidence, the extensive agreement between our results and dynamical simulations requires taking the model seriously.

Appendix: The magnetic exponent

The effect of a random magnetic field applied to the system is obtained by adding to the Hamiltonian (1)

$$\mathcal{H}' = -\sum_i h_i S_i. \tag{A1}$$

We take the random field h_i acting on a spin at site i with z_i neighbours to be the sum of z_i independent terms:

$$h_i = \sum_j^{z_i} h_i^{(j)} \tag{A2}$$

where

$$[h_{(i)}^j]_{\mathrm{av}} = 0 \qquad [(h_i^{(j)})^2]_{\mathrm{av}} = \tfrac{1}{2}\Delta_h. \tag{A3}$$

Thus the last-generation spins, which have coordination number 2, feel a total random field of variance Δ_h, the next-to-last feel a field of variance $2^{d-1}\Delta_h$, and so on. This dependence is the natural generalization of that used in non-random hierarchical models [22].

Let us now examine the renormalization operation in the presence of these external fields. We begin, as always, by tracing over last-generation spins (like S_1 and S_2 in figure 1(b)). As before, the result of each such tracing is a factor in the effective Boltzmann weight $\exp(-\beta H_1)$ associated with the renormalized Hamiltonian. Again, as before, each such factor depends on the untraced spins at the ends of the cell (e.g. S_A and S_C in figure 1(b)). Writing this factor in the form

$$R(S_A, S_C) = \exp[-\beta H_{AC}(S_A, S_C)] \tag{A4}$$

the difference between the zero- and finite-field cases is just that with the field $H_{AC}(S_A, S_C)$ contains terms linear in the spins:

$$-H_{AC}(S_A, S_C) = J'S_AS_C + \delta h_A S_A + \delta h_C S_C + \phi'. \tag{A5}$$

In this way, each of the traced-over spins adds a contribution δh to the field acting on previous-generation spins at the ends of the cell. These contributions can be extracted from

$$-H_{AC}(++) + H_{AC}(--) + H_{AC}(+-) - H_{AC}(-+) = 4\delta h_C \tag{A6}$$

and similarly for δh_A. We can evaluate these terms simply from the result

$$-\beta H_{AC}(S_A, S_C) = \ln R(S_A, S_C) = \ln 2 \cosh \beta(J_{A1}S_A + J_{1C}S_C + h_1) \tag{A7}$$

of tracing out a single spin S_1. For small fields this gives

$$\delta h_C = \tfrac{1}{2}h_1[\tanh \beta(J_{A1} + J_{1C}) + \tanh \beta(J_{A1} - J_{1C})]. \tag{A8}$$

Hence the total field acting on S_C after the renormalization step is the original one (A2) (2^d terms), plus 2^d terms of the form (A8) (one for each bond connecting it with a traced-over spin):

$$h'_C = \sum_{j=1}^{2^d} (h_C^{(j)} + \tfrac{1}{2}h_j \tanh \beta\gamma_+^{(j)} + \tfrac{1}{2}h_j \tanh \beta\gamma_-^{(j)}) \tag{A9}$$

where the $\gamma_\pm^{(j)}$ are the sums (differences) between the two bonds connected to the traced-over spins S_j in the cells to the left and right of S_C. All the terms in (A9) are independent, so the resulting variance is

$$\Delta'_h = 2^{d-1}(1 + [\tanh^2 \beta\gamma]_{av})\Delta_h. \tag{A10}$$

Thus the magnetic exponent (defined in (32)) is

$$y_h = d - 1 + \frac{\ln(1 + [\tanh^2 \beta\gamma]_{av})}{\ln 2}. \tag{A11}$$

In the zero-temperature limit, this just reduces to the exact result $y_h = d$. For $d = 3$ and $T = T_g$ we evaluate numerically the average in (A11) over the fixed point distribution $P^*(J)$ to obtain the value $y_{ch} = 2.65$ used in section 5.

References

[1] Edwards S F and Anderson P W 1975 *J. Phys. F: Met. Phys.* **5** 965
[2] Fisher D S and Huse D A 1986 *Phys. Rev. Lett.* **56** 1601; 1988 *Phys. Rev.* B **38** 386
[3] Parisi G 1980 *J. Phys. A: Math. Gen.* **13** 1101, 1887
[4] Bray A J and Moore M A 1986 *Heidelberg Colloquium on Glassy Dynamics and Optimization* ed L van Hemmen and I Morgenstern (Heidelberg: Springer)
[5] Berker A N and Ostlund S 1979 *J. Phys. C: Solid State Phys.* **12** 4961
[6] Migdal A A 1975 *Zh. Eksp. Teor. Fiz.* **69** 1457 (1975 *Sov. Phys.-JETP* **42** 743)
[7] Kadanoff L P 1976 *Ann. Phys., NY* **100** 359
[8] Young A P and Stinchcombe R B 1976 *J. Phys. C: Solid State Phys.* **9** 4419
[9] Southern B W and Young A P 1977 *J. Phys. C: Solid State Phys.* **10** 2179
[10] Randeria M, Sethna J P and Palmer R G 1985 *Phys. Rev. Lett.* **54** 1321
[11] Grinstein G, Berker A N, Chalupa J and Wortis M 1976 *Phys. Rev. Lett.* **36** 1508
[12] McMillan W L 1984 *J. Phys. C: Solid State Phys.* **17** 3179
[13] Gardner E 1984 *J. Physique* **45** 1755

[14] Sourlas N S 1988 *Europhys. Lett.* **6** 561
[15] Caracciolo S, Parisi G, Patarnello S and Sourlas N 1990 *Europhys. Lett.* **11** 781
[16] Glauber R J 1963 *J. Math. Phys.* **4** 294
[17] Bray A J and Moore M A 1984 *J. Phys. C: Solid State Phys.* **17** L463
[18] McMillan W L 1984 *Phys. Rev.* B **30** 476
[19] Kutasov D, Aharony A, Domany E and Kinzel W 1986 *Phys. Rev. Lett.* **56** 2229
[20] McMillan W L 1984 *J. Phys. C: Solid State Phys.* **17** 3189
[21] Ogielski A T 1985 *Phys. Rev.* B **32** 7384
[22] Griffiths R B and Kaufmann M 1982 *Phys. Rev.* B **26** 5022